Electron kinetic effects on interferometry and polarimetry in high temperature fusion plasmas

2013 Nucl. Fusion 53 113005

(http://iopscience.iop.org/0029-5515/53/11/113005)

IOP Publishing and International Atomic Energy Agency Nuclear Fusion
Nucl. Fusion **53** (2013) 113005 (9pp) doi:10.1088/0029-5515/53/11/113005

Electron kinetic effects on interferometry and polarimetry in high temperature fusion plasmas

V.V. Mirnov[1,3], D.L. Brower[2,3], D.J. Den Hartog[1,3], W.X. Ding[2,3], J. Duff[1] and E. Parke[1]

[1] University of Wisconsin – Madison, Madison, Wisconsin, USA
[2] University of California Los Angeles, Los Angeles, CA, USA
[3] Center for Magnetic Self-Organization in Laboratory and Astrophysical Plasmas, USA

Received 5 February 2013, accepted for publication 22 August 2013
Published 16 September 2013
Online at stacks.iop.org/NF/53/113005

Abstract
At anticipated high electron temperatures in ITER, the effects of electron thermal motion on phase measurements made by the toroidal interferometer/polarimeter (TIP) and poloidal polarimeter (PoPola) diagnostics will be significant and must be precisely treated or the measurement accuracy will fail to meet the specified requirements for ITER operation. We calculate electron thermal corrections to the interferometric phase and polarization state of an electromagnetic wave propagating along tangential and poloidal chords (Faraday and Cotton–Mouton polarimetry) and incorporate them into the Stokes vector equation for evolution of polarization. Although these corrections are small at electron temperatures $T_e \simeq 1$ keV, they become sizable at $T_e \geqslant 10$ keV. The precision of the previous lowest order linear in the $\tau = T_e/m_e c^2$ model may be insufficient; we present a more precise model with τ^2-order corrections to satisfy the high accuracy required for ITER TIP and PoPola diagnostics. Proper treatment of temperature effects will ensure more accurate interpretation of interferometric and polarimetric measurements in fusion devices like ITER and DEMO. The use of precise analytic expressions is especially important for burning plasmas where various interferometric techniques will be used for direct real time feedback control of device operations with time resolution ~1 ms to regulate the rate of the thermonuclear burn and monitor/control the safety factor profile.

1. Introduction

A key issue for advanced optical plasma diagnostics is the gap between the increasing accuracy of the experimental phase measurements by interforometric and polarimetric (I/P) systems and slow progress in the theoretical models used for data analysis and evaluation of the physical quantities of interest. Deficiencies in the models arise from both the insufficient treatment of the physics of laser–plasma interaction and the precision of equilibrium reconstruction methods. This paper addresses the physical issues and investigates the influence of intensive electron thermal motion on propagation of high-frequency electromagnetic waves in magnetically confined plasmas.

Several major laser diagnostics are under development for measurement of plasma density, temperature, magnetic field and current control in ITER: Thomson scattering (TS LIDAR system), toroidal interferometer/polarimeter (TIP) and poloidal polarimeter (PoPola). Each of these measurements is based on the electron response to laser light propagating through the plasma. For a long time, the interpretation of the I/P diagnostics was based on the cold plasma dispersion relation without taking into account corrections caused by the electron thermal motion. This approach starts from derivation of the cold plasma dielectric tensor, the wave dispersion relation and plasma refractive indices. The magnetized plasma exhibits birefringence, and two orthogonal states of wave polarization with different refractive indices are present. Important examples of plasma birefringency are the Faraday (FR) effect of rotation of the polarization plane and the Cotton–Mouton effect (CM) that involves both rotation and deformation of the polarization ellipse [1]. The model which adequately describes these two effects and resulting evolution of polarization in non-uniform plasma and magnetic field is known as the Stokes vector equation. It is derived in the WKB approximation and represented by a differential equation for the three-component unit Stokes vector of polarization which is characterized by the orientation angle and degree of ellipticity of the polarization ellipse.

At anticipated ITER parameters as well as in future burning-pasma devices, the effects of electron thermal motion will be significant and must be accurately treated or the measurements will fail to meet the requirements for basic machine operation and safety. The primary focus of our work is

to examine the effects of electron thermal motion on the plasma dielectric tensor, refractive indices and polarization of high-frequency electromagnetic waves (specifically laser light). We calculate electron thermal corrections to the interferometric phase and polarization state (FR and CM polarimetry) of the wave propagating along both tangential and poloidal chords in ITER and incorporate them into the Stokes vector equation for evolution of polarization. Although these corrections are small at electron temperatures $T_e \simeq 1$ keV, they become sizable at $T_e \geqslant 10$ keV. The use of accurate analytic expressions is especially important for fusion devices like ITER and DEMO where various interferometric techniques will be used not only to determine physical plasma parameters but also for direct real time feedback control of device operations with time resolution ~1 ms to regulate the rate of the thermonuclear burn and also to monitor/control the q profile. This determines the high accuracy (~1%) required for line-averaged interferometry-polarimetry in ITER (see, ITER diagnostic specifications [2]).

Earlier analytical results [3] have already been included in the error analysis and design projections of the ITER TIP and PoPola systems [4, 5]. However, the precision of the previous lowest order linear in $\tau = T_e/m_e c^2$ model [3] may be insufficient; using the same iterative technique we derive now a more precise model with τ^2-order corrections to satisfy the high accuracy required for ITER TIP and PoPola diagnostics. With this model and electron temperature known from Thomson scattering measurements, finite T_e effects can be properly treated. The use of simple analytic expressions is critical for plasma feedback control in real time. Ray tracing codes with fully relativistic dispersion functions and exact temperature dependences can be potentially used for these purposes. However, integrations over velocity space and summation of the Bessel functions required for evaluation of the dielectric tensor elements are computationally intensive and not feasible on ~1 ms time scale. The second order corrections are also important for determination of the limits of applicability of the linear approximation.

This paper is based on the report [6] presented at the IAEA Fusion Energy Conference (2012) in ITER category and devoted to the analysis of advanced optical diagnostics. That report covered two different topics: interferometry/polarimetry (I/P) and Thomson scattering, unified by the importance of relativistic (quadratic in v_{T_e}/c) electron kinetic effects in a high T_e plasma. The present paper focuses on the I/P applications and contains detailed description of this topic. The full treatment of polarization for Thomson scattering, with all derivations and complete multi-parametric analysis of two important polarization characteristics (change of state of polarization and loss of degree of polarization), will be presented in a separate paper now in preparation. Section 2 is devoted to the analytical approach based on the iterative scheme of solution of the relativistic electron kinetic equation. This approach yields the Jones matrix with thermal effects. To the best of our knowledge, the quadratic in τ corrections to the relativistic dielectric tensor of a magnetized plasma have not been calculated previously. They are incorporated into the Stokes vector equation for evolution of polarization with τ^2-accuracy. Brief discussion and conclusions are included in the Summary while the details of calculations are given in appendix A.

2. Electron thermal effects on I/P diagnostics

The ITER TIP system is designed for tangential plasma density measurement from both traditional interferometry and FR polarimetry. It is based on the use of laser beams with the wavelengths 10.6/5.3 μm propagating along five chords in the toroidal plane which are double-passed by retro-reflection from corner cube reflectors mounted in the ITER walls. In a cold plasma, the interferometric phase Φ and the FR rotation angle of polarization ψ_F are proportional to the line integral of the electron density and the line integral of the electron density multiplied by the parallel component of the magnetic field, respectively. For the ITER TIP system parameters, $n \simeq 10^{20}\,\mathrm{m}^{-3}$, $B_\parallel \simeq 5.3$ T, $L \simeq 21$ m, $\lambda = 10.6\,\mu$m, they are as follows:

$$\Phi^{(\mathrm{cold})}\,(\mathrm{rad}) = 2.82 \times 10^{-21}\lambda\,(\mu m) \times \int n_e(z)\,(\mathrm{m}^{-3})\,\mathrm{d}z\,(\mathrm{m}) \simeq 63, \quad (1)$$

$$\psi_F^{(\mathrm{cold})}\,(\mathrm{rad}) = 2.62 \times 10^{-25}\lambda^2\,(\mu\mathrm{m}) \times \int n_e(z)\,(\mathrm{m}^{-3}) B_\parallel(z)\,(\mathrm{T})\,\mathrm{d}z\,(\mathrm{m}) \simeq 0.33. \quad (2)$$

The ITER PoPola diagnostic is based on the FR and CM effects and provides a unique method for measurement of the internal magnetic field and current profile as well as the electron density. It is anticipated to operate with long wavelength far-infrared laser beams (118/50 μm) propagating in the poloidal plane along nine chords via an equatorial port and six chords via an upper port. In this case, with propagation largely perpendicular to the magnetic field, the CM effect becomes significant and leads to a change in the ellipticity characterized by the ellipticity angle χ. For the PoPola system parameters, $n \simeq 10^{20}\,\mathrm{m}^{-3}$, $B_\perp \simeq 5.3$ T, $L \simeq 8$ m, $\lambda = 118\,\mu$m, the induced ellipticity of radiation initially linearly polarized at 45° to $\boldsymbol{B}_\perp$ is given by

$$\chi^{(\mathrm{cold})}\,(\mathrm{rad}) = 2.46 \times 10^{-29}\lambda^3\,(\mu\mathrm{m}) \times \int n_e(z)\,(\mathrm{m}^{-3}) B_\perp^2(z)(\mathrm{T})\,\mathrm{d}z\,(\mathrm{m}) \simeq 0.91. \quad (3)$$

Finite electron temperature effects are neglected when using the cold plasma dispersion relation as given in equations (1)–(3). At high electron temperatures in a fusion plasma, this will lead to significant errors. There are two physically different sources of thermal corrections which are comparable in magnitude but contribute with opposite signs: non-relativistic Doppler-like effects (NR) and the relativistic electron mass dependence on the velocity. The effects of finite electron temperature have been addressed in the non-relativistic limit in [7] where the lowest order linear corrections in τ were calculated on the basis of the non-relativistic dielectric tensor for magnetized plasmas. Our reevaluation of this problem [3] has shown that relativistic effects cannot be ignored. They are also linear in τ, opposite in sign compared to the non-relativistic corrections for the interferometric phase and the FR rotation angle and reduce the magnitude of the thermal correction for the CM effect. The relativistic model combines both non-relativistic Doppler-like and relativistic electron mass effects. According to [3], at $T_e = 25$ keV and $N \simeq 1$, the resulting thermal corrections for Φ, ψ_F, and the CM effect relative to their values in cold plasma

are, respectively, −7.5%, −10% and +22.5%, while the non-relativistic model yields overestimated values , +5%, +15% and +60%, correspondingly.

For formal analysis of electron thermal effects on the I/P diagnostics we have developed an iterative technique of solving the relativistic electron kinetic equation. It is based on the assumption that the wave frequency ω is much higher than the electron cyclotron frequency ω_{ce}. A numerical check on the linear in τ analytical results was performed by using the GENRAY ray tracing code [8] with full relativistic electron dielectric tensor that describes temperature dependences exactly. The results presented in [3] (see figure 5) show good agreement between the analytical model and numerical simulations. The signs of the small deviations observed at high electron temperatures $T_e > 20\,\mathrm{keV}$ are consistent with τ^2 corrections reported below.

Comparison with the experimental results has been made by analysing data from more than 1200 pulses collected during the 2003–2007 period from high-T_e JET discharges. That includes a large number of measurements of induced ellipticity made by the JET poloidal polarimeter and illustrated in figure 4 of [9]. The cold plasma theory was shown to underestimate the induced ellipticity, while the non-relativistic model [7] was shown to overestimate it. Measurements in the range of $3\,\mathrm{keV} < T_e < 12\,\mathrm{keV}$ demonstrated good agreement with the relativistic model [3], confirming the importance of relativistic effects for the evolution of the polarization during high T_e JET discharges. These findings were interpreted by the JET team as the first experimental observation of relativistic effects in plasma polarimetry. Note, the observations were made on the basis of a weak CM effect that required large statistics for reliable identification of the dependence on T_e. Of course, the electron thermal effects are much more pronounced and easily observed for the FR effect, which is much stronger than the CM effect. Thus, the JET experiments have confidently demonstrated the effect of electron thermal motion on plasma polarimetry.

We now present an improved analytic model with quadratic in τ terms that satisfies the 1% accuracy required for the ITER TIP system. For this purpose, we use the kinetic equation to calculate the perturbed electron distribution function and, correspondingly, the linear plasma response as a superposition of currents induced by the electromagnetic wave in plasma. Using these results we calculate the plasma dielectric tensor and analyse electron thermal effects on refractive indices and polarization states of laser light.

Due to the short wavelength of the electromagnetic waves used for plasma diagnostics, their typical frequency ω greatly exceeds the characteristic plasma frequencies such that

$$\omega \gg \omega_{pe} \simeq \omega_{ce} \gg \omega_{ci} \gg \nu_{ei}. \tag{4}$$

Under these conditions, the main contribution to the plasma linear response is given by the electrons while the ion motion can be ignored. Formal theory of linear plasma response is based on the relativistic Vlasov equation for the electron distribution function $F(\boldsymbol{r},\boldsymbol{p},t) = f(\boldsymbol{p}) + \delta f(\boldsymbol{r},\boldsymbol{p},t)$ in a uniform magnetic field $\boldsymbol{B}_0$ which is perturbed by the fast oscillating magnetic and electric field $\boldsymbol{E}$ of the wave. The distribution function is divided into a stationary equilibrium part $f(\boldsymbol{p})$ and a perturbation $\delta f(\boldsymbol{r},\boldsymbol{p},t)$. Presenting $\delta f(\boldsymbol{r},\boldsymbol{p},t)$ as a sum of the Fourier harmonics proportional to $\exp[\mathrm{i}(\boldsymbol{k}\cdot\boldsymbol{r}-\omega t)]$ yields a non-homogeneous differential equation for the Fourier components of δf. Assuming that the unperturbed function is isotropic, this equation in a spherical reference frame (p,θ,ϕ) with the z-axis parallel to $\boldsymbol{B}_0$, $\boldsymbol{p} = p(\sin\theta\cos\phi,\ \sin\theta\sin\phi,\ \cos\theta)$ and $\boldsymbol{k} = k(\sin\alpha,\ 0,\ \cos\alpha)$ takes the form

$$-\mathrm{i}\left(\omega - \frac{\boldsymbol{k}\cdot\boldsymbol{p}}{m_e\gamma}\right)\delta f + \frac{\omega_{ce}}{\gamma}\frac{\partial\delta f}{\partial\phi} = -\frac{e\boldsymbol{E}\cdot\boldsymbol{p}}{p}\frac{\partial f}{\partial p},$$
$$\omega_{ce} = \frac{|e|B_0}{m_e c}, \qquad f(\boldsymbol{p}) = f(|\boldsymbol{p}|) \tag{5}$$

where the relativistic factor γ describes the relationship between particle momentum and velocity, $\boldsymbol{p} = m_e v\gamma$ and α is the angle between $\boldsymbol{k}$ and $\boldsymbol{B}_0$. The same notation $\delta f(\boldsymbol{p})$ is used for the Fourier harmonics of $\delta f(\boldsymbol{p},\boldsymbol{r},t)$. The factor $\gamma = (1 - v^2/c^2)^{-1/2} \equiv (p^2/m_e^2c^2 + 1)^{1/2}$ is also a measure of the relativistic mass increase caused by electron thermal motion that gives rise to the relativistic corrections to the plasma dielectric tensor.

The standard method of solving the kinetic equation (5) is based on the exact integration over ϕ where the constant of integration is determined by the periodicity of δf on ϕ (see, for example, equation (54) in [10]). The exact solution leads to a Bessel function series representation of the dielectric tensor [11]. These expressions should then be expanded over $\tau \ll 1$. Because of the infinite series, resonant factors in the denominator and relatively large value of the argument of the Bessel functions, this presentation is not suitable for the expansion. Instead of the general approach based on the exact solution, we have developed more simple calculation scheme adequate for high-frequency electromagnetic waves with $\omega \gg \omega_{ce}$. It allows us to find finite T_e corrections by means of successive differentiations of standard trigonometric functions. Our approach is based on the recursion relation (7) suggested in [3]. For formal derivation of the recursion relation we introduce a new function $\delta g = \delta f\exp(\Psi)$ where phase function Ψ is defined by the integral

$$\Psi = \mathrm{i}\int_0^\phi \frac{\boldsymbol{k}\cdot\boldsymbol{p}}{m_e\omega_{ce}}\mathrm{d}\phi' = \mathrm{i}q(\phi\cos\alpha\cos\theta + \sin\alpha\sin\theta\sin\phi),$$
$$q = \frac{kp}{m_e\omega_{ce}}. \tag{6}$$

Expressing δf in terms of δg and substituting into the kinetic equation (5) yields a differential equation for δg with a small parameter $\epsilon \ll 1$ and source function R:

$$\delta g = \epsilon\frac{\partial\delta g}{\partial\phi} + R, \qquad R = -\frac{\mathrm{i}e}{p\omega}(\boldsymbol{E}\cdot\boldsymbol{p})\frac{\partial f}{\partial p}\exp\Psi,$$
$$\epsilon = -\frac{\mathrm{i}Y}{\gamma} \ll 1, \tag{7}$$

where standard notation $Y = \omega_{ce}/\omega$ is introduced. This form allows a power series expansion in ϵ where next-order corrections are obtained by differentiating the previous one. The final solution for δf is presented by a series that is a periodic function of ϕ:

$$\delta f = -\frac{\mathrm{i}e}{\omega}\left(\sum_{n=0}\epsilon^n Q_n\right)\frac{\partial f}{\partial p}, \quad Q_n = \exp(-\Psi)\frac{\partial^n}{\partial\phi^n}(\mathcal{E}\exp\Psi),$$
$$\mathcal{E}(\phi) = E_x\sin\theta\cos\phi + E_y\sin\theta\sin\phi + E_z\cos\theta. \tag{8}$$

The recursion procedure is a formal way to derive compact presentation for the series expansion (8). It is equivalent to the expansion of the exact solution [10] in powers of ω_{ce}/ω by means of its successive integration by parts over full differential of the combination $d\phi' \exp(i\gamma\omega\phi'/\omega_{ce})$. Both methods lead to the series expansion illustrated by (A1). The terms containing derivatives of Ψ are proportional to the corresponding powers of $q = kp/(m_e\omega_{ce}) = (N/Y)(p/m_ec)$. This yields a double series expansion in powers of Y and p/m_ec with the convergency conditions $Y \ll 1$, $\tau \ll 1$.

Integrating δf gives the current density $\boldsymbol{j}$ induced in the plasma

$$\boldsymbol{j} = \frac{n_0 e}{m_e}\int_0^\infty \frac{p^3 dp}{\gamma}\int_0^\pi \sin\theta d\theta \int_0^{2\pi}\left(\frac{\boldsymbol{p}}{p}\right) d\phi \delta f(p,\theta,\phi), \tag{9}$$

where n_0 is the equilibrium plasma density. The equilibrium isotropic distribution function $f(p)$ is characterized by a relativistic Maxwellian distribution (normalized to unity)

$$f(p) = \frac{\mu\exp(-\mu\gamma)}{4\pi m_e^3 c^3 K_2(\mu)}, \qquad 4\pi\int_0^\infty f(p)p^2\,dp = 1,$$
$$\mu = 1/\tau = m_e c^2/T_e, \tag{10}$$

where $K_2(\mu)$ is modified Bessel function of the second kind [12]. Using the definition of the displacement vector $\boldsymbol{D}$ and expressing $\boldsymbol{j}$ as a function of the electric field components $E_{x,y,z}$ yields the elements of the dielectric tensor ϵ_{ij}

$$\boldsymbol{D} = \boldsymbol{E} + \frac{4\pi i}{\omega}\boldsymbol{j}, \qquad D_i = \epsilon_{ij}E_j. \tag{11}$$

The angular dependence of δf is described by the Q_n factors. The terms containing derivatives of Ψ are responsible for the appearance of higher powers of p in the equation for δf. Correspondingly, performing integration over p yields higher moments $\langle p^2\rangle$ and $\langle p^4\rangle$ and, thus, forms a power series expansion of the dielectric tensor in $\tau \ll 1$. Integration over angular variables as well as over p is performed analytically with the use of Mathematica [13]. Seven terms in summation over n ($n_{max} = 6$) is enough to obtain the dielectric tensor expanded to second order in τ with all relativistic factors taken into account. These key results (A4) are obtained in the reference frame x', y', z' with z'-axis oriented along $\boldsymbol{B}_0$ and the $\boldsymbol{k}$ vector in the x', z' plane with the angle α between them. As a next step, we transfer the dielectric tensor to the laboratory reference frame x, y, z shown in figure 1 with z axis oriented along $\boldsymbol{k}$ while $\boldsymbol{B}_0$ is arbitrary and has the Cartesian coordinates $B_0(\sin\alpha\cos\beta, \sin\alpha\sin\beta, \cos\alpha)$.

In the WKB approximation, the electric field of the wave is characterized by slowly varying complex amplitude $\boldsymbol{E}$ and fast oscillating phase. The homogeneous system of the Maxwell equations (A8) for three components of $\boldsymbol{E}$ is reduced by expressing E_z in terms of E_x and E_y from the z component of equation (A8). The reduction leads to two coupled equations for E_x and E_y (Jones equations (A13)). Equating the determinant to zero gives two refractive indices N_s^2 and N_f^2 for slow (O-mode) and fast (X-mode) waves, respectively

$$N_{s,f}^2 = \frac{\eta_{xx}+\eta_{yy}}{2} \pm \frac{1}{2}\sqrt{g}, \qquad g = (\eta_{xx}-\eta_{yy})^2 + 4|\eta_{xy}|^2 \tag{12}$$

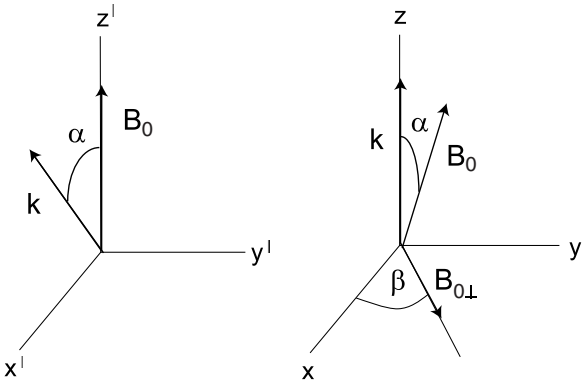

Figure 1. The Stix reference frame $x'y'z'$ with $\boldsymbol{z}' \parallel \boldsymbol{B}_0$ and $\boldsymbol{k}$ in the x', z' plane and the laboratory reference frame x, y, z with $\boldsymbol{z} \parallel \boldsymbol{k}$ and x- and y-axes fixed with respect to the experimental device. The spatially varying azimuth $0 \leqslant \beta \leqslant 2\pi$ is the angle in the x, y plane between $\boldsymbol{x}$ and the direction of $\boldsymbol{B}_{0\perp}$, α is the angle between $\boldsymbol{k}$ and $\boldsymbol{B}_0$.

where 2×2 Jones matrix η_{ik} is defined by (A13). The mean value of N serves as a measure of the interferometric phase Φ (relative to vacuum). The function $\sqrt{g}$ determines the difference between N_s and N_f and, thus, the phase between two normal modes that is a key factor for the evolution of polarization. The polarization is characterized by the polarization factors $\rho_{s,f} = E_y/E_x$:

$$\rho_{s,f} = \frac{\eta_{yy}-\eta_{xx} \pm \sqrt{g}}{2\eta_{xy}}. \tag{13}$$

The phase difference between two normal modes is a function of the plasma parameters $X = \omega_{pe}^2/\omega^2 \ll 1$, $Y = \omega_{ce}/\omega \ll 1$, $\tau = T_e/m_ec^2 \ll 1$, the propagation angle α and the optical path length L. For propagation at an angle α not too close to 90° ($\cos\alpha/Y \gg 1$), the difference between N_s and N_f is linear in Y and leads to the FR rotation of polarization characterized by the phase difference Ψ_F. For the quasi-perpendicular case, $\cos\alpha \ll Y \ll 1$, the difference between two refractive indices is much smaller, $\sim Y^2$, and the polarization evolves according to the CM effect with the corresponding phase difference Θ. Final results for the thermal corrections in uniform plasma and magnetic field are expressed by relative deviations of the functions Φ, Ψ_F and Θ from their cold plasma values $\Phi^{(cold)} = \omega LX/2c$, $\Psi^{(cold)} = \omega LXY/c$, $\Theta^{(cold)} = \omega LXY^2/2c$ (see, for example, appendix A and [1])

$$\Delta\Phi^{(T)}/\Phi^{(cold)} = \tfrac{1}{2}\left(2N^2-5\right)\tau + \tfrac{1}{8}(24N^2-64N^2+55)\tau^2$$
$$\simeq -\tfrac{3}{2}\tau + \tfrac{15}{8}\tau^2,$$
$$\Delta\Psi_F^{(T)}/\Psi_F^{(cold)} = (3N^2-5)\tau + \tfrac{3}{2}(10N^4-23N^2+15)\tau^2$$
$$\simeq -2\tau + 3\tau^2,$$
$$\Delta\Theta^{(T)}/\Theta^{(cold)} = \tfrac{3}{2}(8N^2-5)\tau$$
$$+\tfrac{15}{8}(25-96N^2+72N^4)\tau^2 \simeq \tfrac{9}{2}\tau + \tfrac{15}{8}\tau^2, \tag{14}$$

where $N^2 = 1 - X \simeq 1$. Contributions from the dispersive $\propto(N^2, N^4)$ and non-dispersive terms are strongly amplified by large numerical factors. Since they enter with opposite signs the final coefficients turn out to be of order of unity at $N = 1$. The limit of applicability of the linear approximation is determined by the condition that the second order corrections

are much smaller than the linear terms. Due to cancelations of large numerical factors, this condition yields soft restriction on the electron temperature, $\tau \ll 1$, that does not differ from the original assumption. For $\Delta\Phi^{(T)}$, $\Delta\Psi_F^{(T)}$ linear and quadratic terms in τ have opposite signs and the overall effect is reduced, whereas for $\Delta\Theta^{(T)}$ the terms add to increase the effect. At high electron temperatures $T_e \simeq 20$–50 keV, the quadratic in τ corrections are in the range 0.3–2% for $\Delta\Phi^{(T)}$, $\Delta\Theta^{(T)}$ and between 0.5–3% for $\Delta\Psi_F^{(T)}$. Assuming that overall contribution of all not included in (14) higher order terms is less than 1%, the first two equations for Φ and Ψ_F meet the accuracy (<1%) required for ITER TIP system at $T_e < 30$ keV.

Knowing the electron temperature from Thomson scattering, the thermal effects can be taken into account. To estimate the absolute values of these corrections, note that, for CO_2 laser wavelength $\lambda = 10.6\,\mu$m, the central viewing channel optical path length $L \simeq 21$ m, plasma density $n \simeq 10^{20}\,\mathrm{m}^{-3}$ and $T_e \simeq 30$ keV, the linear correction to the interferometric phase is large (≃0.9 fringes) so that the quadratic correction is also significant (∼24°). Of course, in the TIP case, all plasma parameters in the expressions for Φ and Ψ_F should be modified according to the WKB approximation and treated as line integrated quantities of the form $\int n\,\mathrm{d}z$, $\int nT_e\,\mathrm{d}z$, $\int nT_e^2\,\mathrm{d}z$ and so on.

The use of this standard WKB approach for the polarimetric phases $\Delta\Psi_F^{(T)}$, $\Delta\Theta^{(T)}$ is inappropriate when we are dealing with the data analysis detected by the poloidal polarimeter in ITER. The specific feature of the PoPola system in ITER (and similar diagnostics in other devices) is not only intensive electron thermal motion but also mutual interaction of the FR and CM effects caused by quasi-perpendicular directions of the optical paths in the ITER PoPola system with the coupling factor $Y/\cos\alpha \simeq 0.7$. The origin of the mutual interaction (coupling) is discussed in the Summary. In this situation, the interference of the FR and CM contributions leads to a complicated relation between polarimetric data and line-integrated plasma and magnetic field parameters [5]. Similar complications caused by mutual interaction between between the FR and CM effects have been recently reported by analysing the JET experiments [14]. The model which adequately describes these relations is based on the Stokes vector equation [15, 16]

$$\frac{\mathrm{d}\boldsymbol{s}}{\mathrm{d}z} = \boldsymbol{\Omega} \times \boldsymbol{s}. \tag{15}$$

We use [16] to derive an expression for Ω in terms of Jones matrix elements that is suitable for our analysis

$$\boldsymbol{\Omega} = \frac{\omega}{2c}\left(\eta_{xx} - \eta_{yy},\quad 2\mathcal{R}e\{\eta_{xy}\},\quad 2\mathcal{I}m\{\eta_{xy}\}\right). \tag{16}$$

Equations (15) and (16) describe rotation of the Stokes vector $\boldsymbol{s}$ around the spatially varying angular velocity vector $\boldsymbol{\Omega}$. We are dealing here with fully polarized monochromatic light and ignore absorption, emission and scattering of radiation so that the three-component unit Stokes vector $\boldsymbol{s} = \boldsymbol{S}/S_0$ is used instead of the four-component vector $\boldsymbol{S} = (S_0,\ S_1,\ S_2,\ S_3)$. The position of this vector on Poincare sphere in characterized by the coordinates $\boldsymbol{s} = (\cos 2\chi \cos 2\psi, \cos 2\chi \sin 2\psi, \sin 2\chi)$, where $0 \leqslant \psi \leqslant \pi$ is the azimuth of the polarization ellipse (orientation angle)

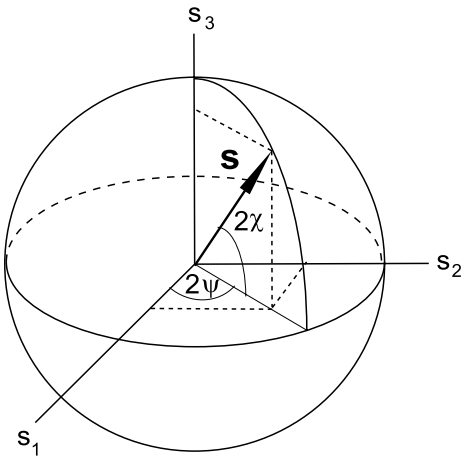

Figure 2. The Cartesian coordinates of the polarization Stokes vector $\boldsymbol{s}$ in terms of angular positions (ψ, χ) on the Poincare sphere.

and $-\pi/4 \leqslant \chi \leqslant \pi/4$ is the ellipticity angle ($\tan\chi = b_2/b_1$) (see figure 2).

Linear in τ relativistic thermal corrections were incorporated in the Stokes vector equation in [3] and used for ITER analysis in [5]. We now present an advanced version of Stokes vector equation with τ^2-order corrections for vector $\boldsymbol{\Omega}$ that determines the polarization dynamics

$$\boldsymbol{\Omega} = \boldsymbol{\Omega}^{(c)} + \frac{T_e}{m_e c^2}\begin{pmatrix} 9\Omega_1^{(c)}/2 \\ 9\Omega_2^{(c)}/2 \\ -2\Omega_3^{(c)} \end{pmatrix} + \left(\frac{T_e}{m_e c^2}\right)^2 \begin{pmatrix} 15\Omega_1^{(c)}/8 \\ 15\Omega_2^{(c)}/8 \\ 3\Omega_3^{(c)} \end{pmatrix},$$

$$\boldsymbol{\Omega}^{(c)} = \frac{\omega}{2c}\begin{pmatrix} XY^2 \sin^2\alpha \cos 2\beta \\ XY^2 \sin^2\alpha \sin 2\beta \\ 2XY \cos\alpha \end{pmatrix}. \tag{17}$$

Equation (17) provides an analytical description that avoids errors caused by finite T_e effects and satisfy ITER accuracy requirements (<1%). Note a misprint (angle ψ instead of β) in the same equation in [6]. The detailed calculations of Ω are presented in appendix A.

3. Summary

Interpretation of polarimetric and interferometric phase measurements in high temperature fusion plasmas differs from that in existing tokamaks due to increased importance of the finite T_e effects. This issue is addressed by solving the relativistic electron kinetic equation and incorporating the results into the Stokes vector equation in the form of precise and simple analytical expressions.

The use of the Stokes vector formalism is important for poloidal polarimetry in tokamak-like magnetic configurations where interpretation of the phase measurements is complicated by mutual interaction of the FR and CM effects due to almost perpendicular to the magnetic field laser beam propagation. Indeed, vector equation (15) can be transformed to two scalar equations for two measured values such as the orientation angle ψ and ellipticity angle χ. This yields exact expressions for $\mathrm{d}\psi/\mathrm{d}z$ and $\mathrm{d}\chi/\mathrm{d}z$ written in terms of the components of $\boldsymbol{\Omega}(z)$ and variables ψ and χ. They show that in addition to pure FR rotation effect (2), the orientation angle ψ has one more term that depends on the ellipticity angle χ while the integrant

of the expression for pure CM effect (3) has an additional factor that depends on ψ. These mutual dependences are often interpreted in the literature as a coupling between FR rotation and CM effect (see, for example, [14]). The Stokes vector equation (15) with accurate temperature corrections (17) allows us to address the issue of the coupling simultaneously with properly accounting for the thermal effects. Preliminary analysis of the thermal effects on the strength of mutual interaction between FR and CM contributions shows that deviation of the FR response from its pure decoupled value increases with T_e while the deviation of the CM response from its decoupled form becomes smaller. More detailed consideration of this question requires sophisticated numerical analysis.

The precise analytical expressions with τ^2-order corrections are derived to satisfy the high accuracy required for ITER diagnostics. At electron temperatures $T_e \simeq 20$–50 keV, the magnitudes of the corresponding quadratic corrections relative to their values in cold plasma are 0.3–2% for Φ and Θ and 0.5–3% for Ψ_F. The absolute values of the τ^2-terms in equation (14) for Φ, Ψ_F and Θ expressed in unites of degree are, respectively, 10.3–67.3°, 0.1–0.6° and 0.15–0.97°. The resolution of the polarimetric diagnostics is determined by the typical system noise level that is reported as ∼0.01° with 250 Hz bandwidth in [17] and ∼0.04° with 20 kHz bandwidth in [18]. It is seen that the quadratic thermal corrections are larger than the resolution of the I/P detectors and, therefore, measurable at sufficiently high T_e.

Linear in τ corrections have been measured in JET [9], but required high statistics due to relatively low T_e (3 keV $< T_e <$ 12 keV) and weak CM effect used for the phase measurements by JET poloidal polarimeter. Quadratic in τ effects on polarimetry are unlikely to be detected on JET or other present day tokamaks/stellarators but will become significant at the higher T_e expected for ITER. However, detecting these effects on interferometry measurements should be feasible on existing devices, where the absolute values of the phases are large and, correspondingly, their quadratic corrections can exceed sensitivity of the detectors.

Our consideration is specifically focused on exact analytical equations for high order thermal corrections and does not take into account other factors (attenuation and dichroism of the laser beam, normal modes coupling in low density boundary layers and so on). These effects can be treated and included in data analysis separately. There are also higher order terms proportional to $Y^2 \ll 1$ and $X \ll 1$ that were omitted in equation (17). Comparing small omitted terms proportional to τ with the factors proportional to τ^2 shows that this is always correct for short wavelength ITER TIP diagnostics. The omitted small terms are less than 10% of τ^2 corrections for the 118 μm PoPola diagnostics at $T_e >$ 15 keV. For the purpose of brevity, the first 'cold' term in equation (17) is shown in lowest in X and Y order. Since exact analytical expression for this factor in cold plasma is well known [7], it is straightforward to improve its accuracy to any desirable order. For example, next order corrections can be taken into account by replacing $\Omega^{(c)}_{1,2} \to \Omega^{(c)}_{1,2}(1 + X + Y^2)$, $\Omega^{(c)}_3 \to \Omega^{(c)}_3(1 + Y^2)$ in the first term of equation (17). Properly accounting for finite temperature effects, both non-relativistic and relativistic, is critical for accurate assessment of planned phase measurements for ITER and future burning plasma experiments. Stokes vector equation with analytical expressions for thermal effects enable one to perform both equilibrium reconstructions [5] (by using I/P signals as input parameters) and feedback control of ITER (or any burning plasma) in real time with fast time resolution by avoiding the need for slowly operating relativistic kinetic ray tracing codes.

Acknowledgments

This work was supported by the US DOE Grant No DE-FC02-05ER54814, the US NSF Cooperative Agreement PHY-0821899 Center for Magnetic Self-Organization in Laboratory and Astrophysical Plasmas and the US ITER Project Office. We acknowledge useful discussions with staff members of the MST experiment and members of the University of Wisconsin Center for Plasma Theory and Computation.

Appendix A. Temperature corrections to the I/P properties

The angular dependence of δf is determined by the Q_n factors. A typical structure of Q_n is illustrated by the first five terms of the series (8) (up to ϵ^4 order)

$$\begin{aligned}\delta f(p,\theta,\phi) \propto \underline{\mathcal{E}} + \epsilon[\underline{\mathcal{E}'} + \mathcal{E}\Psi'] + \epsilon^2[\underline{\mathcal{E}''} + 2\mathcal{E}'\Psi' + \mathcal{E}(\underline{\Psi'^2} + \Psi'')] \\ + \epsilon^3[\underline{\mathcal{E}'''} + 3\mathcal{E}''\Psi' + 3\mathcal{E}'(\Psi'' + \underline{\Psi'^2}) + \mathcal{E}(\Psi'^3 + 3\underline{\Psi'\Psi''} + \Psi''')] \\ + \epsilon^4[\underline{\mathcal{E}''''} + 4\mathcal{E}'''\Psi' + 6\mathcal{E}''(\Psi'' + \underline{\Psi'^2}) + 4\mathcal{E}'(\Psi'^3 + 3\underline{\Psi'\Psi''} + \Psi''') \\ + \mathcal{E}(\underline{\Psi'^4} + 6\Psi'^2\Psi'' + 3\underline{\Psi''^2} + 4\underline{\Psi'\Psi'''} + \Psi'''')].\end{aligned} \tag{A1}$$

The terms containing derivatives of Ψ are proportional to the corresponding powers of $q = kp/(m_e\omega_{ce})$. The angular dependences of δf are presented by the products of the trigonometric functions of ϕ and θ. Additional angular dependences appear in (9) due to unit vector $\boldsymbol{p}/p = (\sin\theta\cos\phi,\ \sin\theta\sin\phi,\ \cos\theta)$. Integrating (9) over θ and ϕ analytically with the use of Mathematica shows that only even powers of q contribute to $\boldsymbol{j}$ while terms with odd powers cancel after integration. To illustrate this properties all non-vanishing terms are underlined in (A1). Integration over angular variables results in a vector $\langle \boldsymbol{Q} \rangle$ obtained as a function of p or, equivalently, γ

$$\langle \boldsymbol{Q} \rangle(\gamma) = \sum_{n=0} \epsilon^n \int_0^\pi \sin\theta \mathrm{d}\theta \int_0^{2\pi} \left(\frac{\boldsymbol{p}}{p}\right) Q_n \mathrm{d}\phi. \tag{A2}$$

The relativistic factor γ is used instead of p for integration in equation (9). Vector $\langle \boldsymbol{Q} \rangle$ is integrated over γ with the use of variable of integration $\xi = \mu(\gamma - 1)$, $0 \leqslant \xi \leqslant \infty$

$$\begin{aligned}\boldsymbol{j} = \frac{i n_0 e^2}{m_e \omega} \frac{\exp(-\mu)}{4\pi\mu^{1/2} K_2(\mu)} \int_0^\infty \mathrm{d}\xi \frac{(2+\xi\tau)^{3/2}}{1+\xi\tau} \xi^{3/2} \\ \times \exp(-\xi)\langle \boldsymbol{Q} \rangle(\xi\tau).\end{aligned} \tag{A3}$$

Expanding the integrand and the vector $\langle \boldsymbol{Q} \rangle(\xi\tau)$ in powers of $\tau \ll 1$ results in functions of ξ which are further integrated analytically. This yields elements of the dielectric tensor ϵ'_{ij} with τ^2 thermal corrections in the reference frame x', y', z' (with z'-axis along $\boldsymbol{B}_0$ and vector $\boldsymbol{k}$ in the x'–z' plane). To provide τ^2 accuracy seven terms were taken in the sum (8)

(up to ϵ^6 order). Contrary to the case of cold electrons, all six elements of the Hermitian tensor ϵ'_{ij} ($\epsilon'_{ij} = \epsilon'^{\star}_{ji}$) are non-zero

$$\begin{aligned}
\epsilon'_{xx} &= 1 - X(1+Y^2) + \tau X\left(N^2\cos(2\alpha) + \frac{9}{2}N^2Y^2\cos(2\alpha)\right.\\
&\left. -\frac{21}{2}N^2Y^2 - 2N^2 + \frac{15Y^2}{2} + \frac{5}{2}\right) + \tau^2 X\left(6N^4\cos(2\alpha)\right.\\
&\left. +\frac{165}{2}N^4Y^2\cos(2\alpha) - \frac{15}{4}N^4Y^2\cos(4\alpha) - \frac{495}{4}N^4Y^2\right.\\
&\left. -9N^4 - 8N^2\cos(2\alpha) - \frac{135}{2}N^2Y^2\cos(2\alpha) + \frac{315N^2Y^2}{2}\right.\\
&\left. +16N^2 - \frac{375Y^2}{8} - \frac{55}{8}\right),\\
\epsilon'_{xy} &= \mathrm{i}XY\left[1 + \tau\left(-\frac{3}{2}N^2\cos(2\alpha) + \frac{9N^2}{2} - 5\right)\right.\\
&\left. +\tau^2\left(-15N^4\cos(2\alpha) + 30N^4 + \frac{69}{4}N^2\cos(2\alpha)\right.\right.\\
&\left.\left. -\frac{207N^2}{4} + \frac{45}{2}\right)\right],\\
\epsilon'_{xz} &= XN^2\sin(2\alpha)\left[-\tau\left(1+2Y^2\right) + \tau^2\left(\frac{15}{2}N^2Y^2\cos(2\alpha)\right.\right.\\
&\left.\left. -\frac{75}{2}N^2Y^2 - 6N^2 + 30Y^2 + 8\right)\right],\\
\epsilon'_{yy} &= 1 - X(1+Y^2) + X\tau\left(\frac{7}{2}N^2Y^2\cos(2\alpha) - \frac{19}{2}N^2Y^2\right.\\
&\left. -N^2 + \frac{15Y^2}{2} + \frac{5}{2}\right)\\
&+X\tau^2\left(\frac{285}{2}N^2Y^2 + \frac{105}{2}N^4Y^2\cos(2\alpha) - \frac{195}{2}N^4Y^2\right.\\
&\left. -3N^4 - \frac{105}{2}N^2Y^2\cos(2\alpha) + 8N^2 - \frac{375Y^2}{8} - \frac{55}{8}\right),\\
\epsilon'_{yz} &= -\mathrm{i}XYN^2\sin(2\alpha)\left[\left(15N^2 - \frac{69}{4}\right)\tau^2 + \frac{3\tau}{2}\right],\\
\epsilon'_{zz} &= 1 - X + \tau X\left(-N^2\cos(2\alpha) + \frac{1}{2}N^2Y^2\cos(2\alpha)\right.\\
&\left. -\frac{1}{2}N^2Y^2 - 2N^2 + \frac{5}{2}\right) + \tau^2 X\left(-6N^4\cos(2\alpha)\right.\\
&\left. +\frac{15}{2}N^4Y^2\cos(2\alpha) + \frac{15}{4}N^4Y^2\cos(4\alpha) - \frac{45}{4}N^4Y^2\right.\\
&\left. -9N^4 + 8N^2\cos(2\alpha) - \frac{15}{2}N^2Y^2\cos(2\alpha)\right.\\
&\left. +\frac{15}{2}N^2Y^2 + 16N^2 - \frac{55}{8}\right). \qquad \text{(A4)}
\end{aligned}$$

The main purpose of this work is a rigorous expansion in powers of τ, and, correspondingly, only dominant terms of order Y^2 ($Y = \omega_{ce}/\omega \ll 1$) and lower are kept in (A4). This is the lowest order needed for correct evaluation of the I/P responses. Since they are calculated in linear approximation in X ($X = \omega_{pe}^2/\omega^2 \ll 1$), the refractive index should formally be set to $N^2 = 1$ in rhs of (A4). However, because of computational convenience we treat N^2 as an arbitrary parameter in intermediate equations and put $N^2 = 1$ in the final expressions.

The correctness of (A4) is checked by comparison with some known limiting cases. As a test, we use [19], devoted to a fully relativistic dielectric tensor in a plasma without a magnetic field. The dielectric tensor of a non-magnetized plasma is isotropic and characterized by its longitudinal ϵ_L and transversal ϵ_T components

$$\epsilon_{ij} = \epsilon_T\left(\delta_{ij} - \frac{k_i k_j}{k^2}\right) + \epsilon_L\frac{k_i k_j}{k^2}, \qquad \text{(A5)}$$

where ϵ_L and ϵ_T are functions of the absolute value $|\boldsymbol{k}| = k$ only. Solving (A5) for ϵ_T and ϵ_L

$$\epsilon_L = \epsilon_{ij}\frac{k_i k_j}{k^2}, \qquad \epsilon_T = \frac{1}{2}\epsilon_{ij}\left(\delta_{ij} - \frac{k_i k_j}{k^2}\right) \qquad \text{(A6)}$$

allow us to calculate these two functions from (A4). Putting $Y = 0$ in (A4) for limiting transition to zero magnetic field and taking $\boldsymbol{k} = (k\sin\alpha,\ 0,\ k\cos\alpha)$ yields

$$\begin{aligned}
\epsilon_T &= 1 - X + \tau X\left(\frac{5}{2} - N^2\right) - \tau^2 X\left(3N^4 - 8N^2 + \frac{55}{8}\right),\\
\epsilon_L &= 1 - X - \tau X\left(3N^2 - \frac{5}{2}\right)\\
&\quad -\tau^2 X\left(15N^4 - 24N^2 + \frac{55}{8}\right). \qquad \text{(A7)}
\end{aligned}$$

These factors, indeed, are the functions of $N^2 = k^2c^2/\omega^2$ only (the angular dependences on α cancel). The specific dependences on k are consistent with the weakly relativistic limit of the corresponding non-magnetized expressions in [19]. Since the wave length of the laser light is short and the effects caused by the magnetic field are small, the dielectric constant ϵ_T can be used for interpretation of the interferometric measurements. The dispersion relation, $N^2 = \epsilon_T$, determines k value in plasma and the interferometric phase compared to vacuum $\Phi = (k_v - k)L$. Relative deviation of this phase $\Delta\Phi^{(T)}$ from its cold value $\Phi^{(c)} = X\omega L/2c$ is caused by the finite electron temperature effects. The corresponding linear and quadratic corrections in uniform plasma are given by the first equation (14).

Based on the well checked dielectric tensor (A4), we now analyse the case of propagation in magnetized plasma ($Y \neq 0$). First, consider two specific propagation directions in uniform plasma and magnetic field: pure parallel $\alpha = 0$ and perpendicular $\alpha = \pi/2$. The homogeneous system of the Maxwell equations

$$\left(\delta_{ij}N^2 - n_i n_j N^2 - \epsilon'_{ij}\right)E_j = 0, \qquad \boldsymbol{n} = \boldsymbol{k}/k,$$
$$i, j = 1, 2, 3 \qquad \text{(A8)}$$

determines the dispersion and the polarization properties of the waves. In $\alpha = 0$ case, $\boldsymbol{k} = (0,\ 0,\ k)$ and $\epsilon'_{xx} = \epsilon'_{yy} = \epsilon_\perp$, $\epsilon'_{xz} = \epsilon'_{yz} = \epsilon'_{zx} = \epsilon'_{zy} = 0$. The dispersion relation for two circularly polarized normal waves, $E_x = \pm E_y$, reads $N^2 = \epsilon_\perp \pm |\epsilon'_{xy}|$. This determines the difference between two refraction indices $N_s - N_f = |\epsilon'_{xy}|$ and corresponding phase Ψ_F between slow and fast waves that leads to the FR rotation of the polarization plane. Putting $\alpha = 0$ in ϵ'_{xy}, yields relative deviation of this phase $\Delta\Psi_F^{(T)}$ from its cold plasma value $\Psi_F^{(c)} = XY\omega L/c$. Linear and quadratic thermal corrections to the FR phase are presented by the second equation (14).

In $\alpha = \pi/2$ case, $\boldsymbol{k}$= (k, 0, 0) while $\epsilon'_{xz} = \epsilon'_{yz} = \epsilon'_{zx} = \epsilon'_{zy} = 0$. Then, the x-component of (A8) results in the relation, $E_x = -\epsilon'_{xy}E_y/\epsilon'_{xx}$ showing that $E_x \simeq XYE_y \ll E_y$. Ignoring small ($\propto X^2$) contribution of this component to two other projections of (A8), yields two decoupled equations for E_y and E_z

$$\left(N^2 - \epsilon'_{yy}\right) E_y = 0, \qquad \left(N^2 - \epsilon'_{zz}\right) E_z = 0. \tag{A9}$$

Thus, there are two linearly polarized fast and slow normal modes with the refraction indices $N_s^2 = \epsilon'_{zz}$ and $N_f^2 = \epsilon'_{yy}$, respectively. The difference of the refractive indices $N_s - N_f = (\epsilon'_{zz} - \epsilon'_{yy})/2$ is proportional to XY^2. The phase between two normal modes leads to the change of ellipticity, and the polarization evolves according to the CM effect. Calculating $\epsilon'_{zz} - \epsilon'_{yy}$ with $\alpha = \pi/2$, yields relative deviation of the CM phase $\Delta\Theta^{(T)}$ from its cold plasma value $\Theta^{(c)} = XY^2\omega L/2c$. Linear and quadratic finite electron temperature corrections to the CM phase are presented by the third equation (14).

In the general case of non-uniform plasma and magnetic field varying spatially on a scale $L \gg \lambda/2\pi$, the evolution of polarization is described by the WKB formalism and expressed by the Stokes vector equation (15). In order to calculate $\boldsymbol{\Omega}$, we take equations (71)–(73) from [16] and express $\boldsymbol{\Omega}$ as a function of the Jones matrix elements. To perform these transformations, we use (13) to derive the following relationships

$$\begin{aligned}
1 - \rho_s\rho_s^\star &= -\frac{(\eta_{yy} - \eta_{xx})(\eta_{yy} - \eta_{xx} + \sqrt{g})}{2|\eta_{xy}|^2},\\
1 + \rho_s\rho_s^\star &= \frac{\sqrt{g}(\eta_{yy} - \eta_{xx} + \sqrt{g})}{2|\eta_{xy}|^2},\\
\rho_s + \rho_s^\star &= \frac{(\eta_{yy} - \eta_{xx} + \sqrt{g})\mathcal{R}e\{\eta_{xy}\}}{|\eta_{xy}|^2},\\
\rho_s^\star - \rho_s &= \frac{\mathrm{i}(\eta_{yy} - \eta_{xx} + \sqrt{g})\mathcal{I}m\{\eta_{xy}\}}{|\eta_{xy}|^2},
\end{aligned} \tag{A10}$$

where factor g is determined by (12), the Jones matrix elements η_{ik} are defined by (A13). Substituting (A10) to (71)–(73) (note, that the factor (−i) is missed in (73)) and taking into account that $N_s - N_f = \sqrt{g}/2$ in linear in X approximation, yields three components of $\boldsymbol{\Omega}$:

$$\boldsymbol{\Omega} = \frac{\omega}{2c}\left(\eta_{xx} - \eta_{yy}, \quad 2\mathcal{R}e\{\eta_{xy}\}, \; 2\mathcal{I}m\{\eta_{xy}\}\right). \tag{A11}$$

Equation (A11) is consistent with equation (20) in [20] except opposite sign of Ω_1 and Ω_2 caused by different definition of s_3. This universal form is suitable for further calculations because of straightforward relation between η_{ij} and already known elements (A4). Indeed, the Jones matrix is determined by the dielectric tensor ϵ'_{ij} transferred to the laboratory reference frame x, y, z introduced in section 2 (see figure 1). The transformation is achieved by two successive rotations of the initial reference frame around the y' axis by the angle α and around the z' axis by the angle $\pi - \beta$. The tensor ϵ_{ij} is related to ϵ'_{ij} as follows

$$\begin{aligned}
\boldsymbol{\epsilon} &= \boldsymbol{T}\cdot\boldsymbol{\epsilon}'\cdot\boldsymbol{T}^{-1},\\
\boldsymbol{T} &= \begin{pmatrix} -\cos\alpha\cos\beta & \sin\beta & \sin\alpha\cos\beta\\ -\cos\alpha\sin\beta & -\cos\beta & \sin\alpha\sin\beta\\ \sin\alpha & 0 & \cos\alpha \end{pmatrix},
\end{aligned} \tag{A12}$$

where $\boldsymbol{T}$ is the transformation matrix. Expressing E_z in terms of E_x and E_y from the z component of (A8) and substituting into the x and y components yields two coupled equations for E_x and E_y (Jones equations)

$$\begin{aligned}
&\begin{pmatrix} N^2 - \eta_{xx} & -\eta_{xy}\\ -\eta_{yx} & N^2 - \eta_{yy} \end{pmatrix}\begin{pmatrix} E_x\\ E_y \end{pmatrix} = 0,\\
&\eta_{ij} = \epsilon_{ij} - \epsilon_{iz}\epsilon_{zj}/\epsilon_{zz}, \quad i, j = 1, 2.
\end{aligned} \tag{A13}$$

All tensors ϵ'_{ij}, ϵ_{ij} and η_{ij} are Hermitian. Following linear in $X \ll 1$ approximation, we drop small factors $\epsilon_{iz}\epsilon_{zj}/\epsilon_{zz} \propto X^2$ and set $\eta_{xx} = \epsilon_{xx}$, $\eta_{yy} = \epsilon_{yy}$, $\eta_{xy} = \epsilon_{xy}$. For illustration, we show the results of calculations of the off-diagonal element η_{xy}. Although initial element ϵ'_{xy} is purely imaginary, the transformed element η_{xy} is a complex number

$$\begin{aligned}
\eta_{xy} = &\frac{\mathrm{i}}{2}XY\cos(\alpha)(\tau(30N^4\tau + N^2(6 - 69\tau) + 5(9\tau - 2)) + 2)\\
&+\frac{1}{16}XY^2\sin^2(\alpha)\sin(2\beta)(3\tau(8N^2(15(3N^2 - 4)\tau + 4)\\
&+5(25\tau - 4)) + 8).
\end{aligned} \tag{A14}$$

Due to its complex structure, the off-diagonal element η_{xy} provides non-zero $\Omega_2 \propto \sin^2\alpha\sin 2\beta$ and $\Omega_3 \propto \cos\alpha$ components. All three components of $\boldsymbol{\Omega}$ are as follows:

$$\begin{aligned}
\Omega_1 = &XY^2\sin^2\alpha\cos 2\beta\left(1 + \frac{1}{8}(96N^2 - 60)\tau\right.\\
&\left.+\frac{1}{8}(360(3N^2 - 4)N^2 + 375)\tau^2\right)\frac{\omega}{2c},\\
\Omega_2 = &XY^2\sin^2\alpha\sin 2\beta\left(1 + \frac{1}{8}(96N^2 - 60)\tau\right.\\
&\left.+\frac{1}{8}(360(3N^2 - 4)N^2 + 375)\tau^2\right)\frac{\omega}{2c},\\
\Omega_3 = &XY\cos\alpha\left(1 + \frac{1}{2}\left(6N^2 - 10\right)\tau\right.\\
&\left.+\frac{1}{2}\left(30N^4 - 69N^2 + 45\right)\tau^2\right)\frac{\omega}{c}.
\end{aligned} \tag{A15}$$

Setting $N^2 = 1$ in lowest linear in X order, yields the Stokes vector equation (15) with linear and quadratic in τ thermal corrections (17).

References

[1] Hutchinson I.H. 2001 *Principles of Plasma Diagnostics* (Cambridge: Cambridge University Press)
[2] Donne A.J.H. *et al* 2007 *Nucl. Fusion* **47** S337–84
[3] Mirnov V.V., Ding W.X., Brower D.L., Van Zeeland M.A., and Carlstrom T.N. 2007 *Phys. Plasmas* **14** 102105
[4] Van Zeeland M.A. *et al* 2013 *Rev. Sci. Instrum.* **84** 043501
[5] Imazawa R., Kawano Y. and Kusama Y. 2011 *Nucl. Fusion* **51** 113022
[6] Mirnov V.V., Brower D.L., Den Hartog D.J., Ding W.X., Duff J. and Parke E. *Proc. 24th Int. Conf. on Fusion Energy 2012 (San Diego, CA, 2012)* (Vienna: IAEA) CD-ROM file ITR/P5-32 and http://www-naweb.iaea.org/napc/physics/FEC/FEC2012/index.htm
[7] Segre S.E. and Zanza V. 2002 *Phys. Plasmas* **9** 2919
[8] Smirnov A.P. and Harvey R.W. 1994 *Bull. Am. Phys. Soc.* **39** 1626
[9] Ford O.P., Svensson J., Boboc A., McDonald D.C. and JET EFDA contributors 2009 *Plasma Phys. Control. Fusion* **51** 065004

[10] Oraevsky V.N. 1989 Handbook of Plasma Physics *Basic Plasma Physics* vol 1, 2, ed A.A. Galeev and R.N. Sudan (New York: Elsevier) p 95
[11] Brambilla M. 1998 *Kinetic Theory of Plasma Waves* (Oxford: Clarendon) p 135
[12] Abramowitz M. and Stegun I.A. 1964 *Handbook of Mathematical Functions* (Washington, DC: National Bureau of Standards) p 374
[13] Wolfram Research, Inc. 2010 *Mathematica* Version 8.0 (Champaign, IL: Wolfram Research Inc.)
[14] Orsitto F.P., Boboc A., Gaudion P., Gelfusa M., Giovannozzi E., Mazotta C., Murari A. and JET-EFDA Contributors 2010 *Rev. Sci. Instrum.* **81** 10D533
[15] Segre S.E. 1999 *Plasma Phys. Control. Fusion* **41** R57
[16] Segre S.E. and Zanza V. 2011 *Phys. Plasmas* **18** 092107
[17] Kawano Y., Chiba S. and Inoue A. 2001 *Rev. Sci. Instrum.* **72** 1068
[18] Brower D.L. *et al* 2003 *Rev. Sci. Instrum.* **74** 1534
[19] Bergman J. and Elliason B. 2001 *Phys. Plasmas* **8** 1482
[20] Kravtsov Yu.A., Bieg B. and Bliokh, K.Yu. 2007 *J. Opt. Soc. Am.* A **24** 3388